Modulational instability and impact of potassium leakage on Nerve Pulse Propagation in a Weakly Dissipative Myelinated Axon

Arnaud Djine[1]*and Serge Bruno Yamgoué[2]

[1]Department of Physics, Faculty of Science, University of Bamenda,

Po. Box 39 Bamenda, Cameroon

[3]Department of Physics, Higher Teacher Training College Bambili,The University of Bamenda, P.O. Box 39 Bamenda Cameroon

May 9, 2026

Abstract

In this paper, we investigate the impact of ionic leakage currents and perform a modulational instability analysis in a weakly dissipative myelinated axon. Using the well-known FitzHugh–Nagumo equation, we derive a generalized discrete nonlinear lattice equation, from which the dispersion relation and group velocity are obtained, allowing us to examine the influence of leakage. Applying the reductive perturbation method, we derive a cubic complex Schrödinger equation, followed by a modulational instability analysis. An ansatz is introduced to obtain exact solutions, and by direct integration, solitary wave solutions are explicitly obtained, including bright and dark solitons, as well as a periodic solution. The effect of potassium ion leakage is clearly reflected in these solutions, significantly affecting the amplitude of the solitons. Finally, numerical simulations using the finite difference method are performed, showing excellent agreement with the analytical results.

Keywords: Potassium leakage; FitzHugh-Nagumo Model; Reductive perturbation; Solitary waves.

1 Introduction

Wave propagation and pattern formation in excitable media have long been central topics in the study of nonlinear dynamical systems [1, 2] with important applications in biology, chemistry, and physics [3, 4]. These phenomena are commonly described within the framework of reaction–diffusion equations [5, 6], which provide a powerful setting for analyzing spatiotemporal evolution in complex media. Among the simplest and most widely used models in this context is the two-variable FitzHugh–Nagumo (FHN) model [7, 8]. Originally introduced as a reduced version of the Hodgkin–Huxley model [9], the FHN system retains

*Corresponding author. E-mail: arnauddjine@gmail.com

the essential nonlinear mechanisms governing excitability while remaining mathematically tractable. In particular, it captures the interaction between a fast excitation variable, associated with the membrane potential, and a slower recovery variable that regulates ionic processes [10]. Through this interplay, the model reproduces key qualitative features such as threshold activation, pulse propagation, and refractory behavior [11, 12]. More recently, several extensions of the FHN framework, including fractional-order, stochastic, and network-based formulations, have been proposed to better account for memory effects and complex neuronal interactions [13, 14, 15].

From a physiological viewpoint, nerve impulses (action potentials) correspond to rapid and transient variations of the electrical potential across neuronal membranes [16], driven primarily by the controlled movement of sodium (Na^+) and potassium (K^+) ions [17]. In myelinated nerve fibers, the presence of the myelin sheath, periodically interrupted at the nodes of Ranvier, gives rise to saltatory conduction [18], whereby the signal effectively jumps from node to node. This mechanism significantly enhances conduction velocity and efficiency [19]. Consequently, the discrete structure of myelinated axons provides a natural basis for the development of spatially discrete models that more accurately reflect the underlying physiological architecture.

When the FHN model is formulated in a spatially discrete setting, the resulting dynamical behavior becomes considerably richer than in continuous systems [20]. In particular, discrete media exhibit intrinsic properties that vanish in the continuum limit. A notable example is the existence of a critical coupling threshold required for successful wave propagation; below this threshold, propagation failure occurs, whereas continuous systems may support propagation for arbitrarily small coupling strengths [11, 21, 22]. This phenomenon has been the subject of numerous investigations. For instance, Booth *et al.* [21] studied front propagation under slow recovery conditions, while Hastings *et al.* [23] analyzed travelling wave solutions in related excitable systems. More recent studies have further highlighted the influence of discreteness, coupling strength, and network structure on synchronization, stability, and wave interactions in neuronal systems [24, 25].

Dissipation represents another key factor influencing nerve impulse propagation. In biological systems, dissipative effects arise naturally from ionic leakage currents, membrane resistance, and metabolic energy losses [26], leading to nonequilibrium spatiotemporal dynamics [27, 28, 29]. These effects can significantly alter wave behavior; for example, propagating pulses may attenuate, deform, or even disappear after interactions in the absence of sustained energy input [30, 31]. Nevertheless, localized excitations resembling soliton-like structures have been observed in various nonlinear systems, including optical and neural media [32, 33, 34]. In addition, modern theoretical approaches, including statistical and field-theoretic descriptions, have provided deeper insight into the collective behavior of excitable systems and neural signal propagation [35].

Despite the extensive body of literature on excitable systems, an important aspect remains insufficiently explored. In many existing studies, the effect of ionic leakage currents is either neglected or treated as a

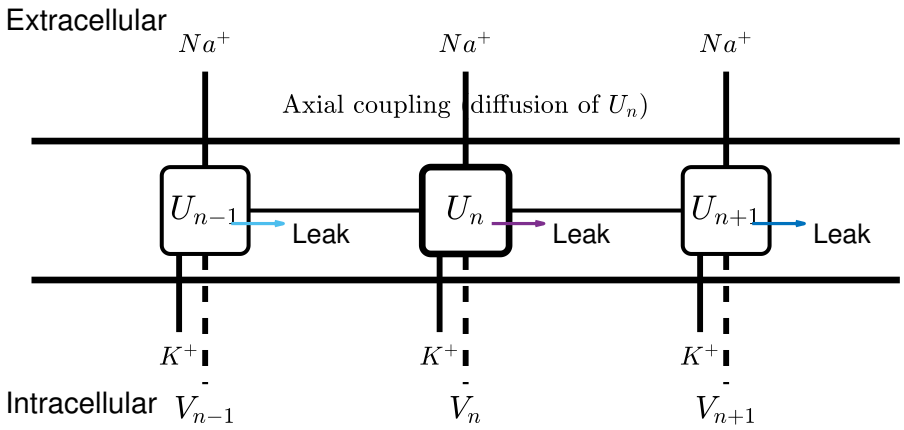

Figure 1: Discrete nerve axon model showing membrane potentials U_n coupled to neighboring nodes and associated recovery variables V_n, consistent with the FitzHugh-Nagumo dynamics.

small perturbation [36, 37, 38]. However, from both physical and physiological perspectives, leakage currents constitute an intrinsic dissipative mechanism that can significantly influence wave propagation, stability, and energy balance [39]. Motivated by these considerations, the present work investigates the impact of ionic leakage current on pulse propagation in a weakly dissipative, spatially discrete FitzHugh–Nagumo model describing a myelinated nerve axon.

Unlike previous studies that either neglect ionic leakage or treat it as a small perturbation, the present work explicitly incorporates potassium leakage as a key dissipative parameter in a discrete FitzHugh–Nagumo framework. This allows us to systematically analyze its influence on dispersion properties, modulational instability, and nonlinear wave structures. In particular, we show how leakage modifies both the amplitude and stability of soliton solutions, providing new insights into the role of dissipation in discrete excitable systems.

2 Model description and equations

In this section, we present the model equation. It is a one-dimensional chain described by FitzHugh-Nagumo equation as:

$$\frac{du_n}{dt} = u_n - \frac{u_n^3}{3} - v_n + K\left(u_{n+1} - 2u_n + u_{n-1}\right) \tag{1a}$$

$$\frac{dv_n}{dt} = a + bu_n - cv_n \tag{1b}$$

In Eq.(1), the variables u_n and v_n are respectively the membrane potential and the recovery variable at exactly the n^{th} excitable membrane site known as Ranvier node. As shown in Fig. 1, these quantities are represented at each discrete node, where u_n appears as the local membrane potential and v_n is shown as the associated recovery variable. The recovery variable governs the slow evolution of the system, as the small parameters $a, b, c \ll 1$ induce only gradual changes over time. This slow dynamics is illustrated by the vertical connections associated with v_n. In Eq.(1a), the term u_n characterizes the positive feedback effect, whereby membrane depolarization stimulates further depolarization through the activation of voltage-gated

sodium channels [36, 37]. . In contrast, the term $-u_n^3/3$ represents a rapid negative feedback mechanism arising from the self-inactivation of the sodium channels, which acts to suppress the depolarization [7, 8, 36]. These processes are schematically represented by the ionic currents across the membrane. The third term $-v_n$ describes a recovery mechanism that can be physically interpreted as the regulation of outward potassium currents, which act to oppose membrane depolarization. This effect is also indicated through the outward ionic pathways in the diagram. The final term denotes the discrete diffusive coupling, with coupling coefficient K, and is proportional to the difference in internodal currents across a specific node of Ranvier. This interaction is depicted by the horizontal connections linking the neighboring nodes u_{n-1}, u_n, and u_{n+1}, as seen in Fig. 1. The first term in Eq.(1b), namely a, primarily represents the potassium leakage current, illustrated by the leak pathways across the membrane. The term bu_n describes the activation of voltage-gated potassium channels by the membrane potential u_n, which leads to an increase in the magnitude of v_n. Finally, the term $-cv_n$ represents the active pumping mechanism responsible for the removal of potassium ions from the neuron. To progress in the study, the first derivative with respect to time of Eq.(1a) is taken and then, the term $\dot{v}_n$ is replaced by the right hand side of Eq.(1b). To completely eliminate v_n in this new equation, we employ the first equation (1a) and the result yields.

$$\begin{aligned}\frac{d^2u_n}{dt^2}+\gamma_1 u_n^3+u_n^2\frac{du_n}{dt}+{\Omega_0}^2u_n+\gamma_2\frac{du_n}{dt}+\gamma_0 &= D_0\left(u_{n+1}-2u_n+u_{n-1}\right)\\ &\quad+D_1\left(\frac{du_{n+1}}{dt}-2\frac{du_n}{dt}+\frac{du_{n-1}}{dt}\right)\end{aligned} \tag{2}$$

where

$$\gamma_1=\frac{1}{3}c,\ \ \gamma_2=c-1,\ \ \Omega_0^2=b-c,\ \ \gamma_0=a,\ \ D_0=cK,\ \ D_1=K \tag{3}$$

are all constants. Eq.(2) represents the Liénard formulation of the FitzHugh-Nagumo model for a myelinated nerve fiber, which can be regarded as a modified variant of the Van der Pol equation. Vanishing the constants $\{D_0, D_1\}$, one remarks that, Eq.(2) is a cubic Liénard-type equation with linear damping, which is often interpreted as an extension of the classical damped oscillator. In the limiting case where the system operates within the linear regime and dissipative effects are neglected, the equation reduces to the well-known linear harmonic oscillator, a fundamental model with extensive applications in both classical and quantum physics. Equations of the Liénard class have been widely explored from mathematical as well as physical viewpoints, and they continue to attract significant attention as an active area of research in mathematical physics[40, 41, 42, 43].

Examining Equation (2), one notes that substituting a constant into the equation leads to an inconsistency: the left-hand side becomes a nonzero constant, whereas the right-hand side reduces to zero. To address this discrepancy, a change of variables is introduced, which allows the formulation to properly account for this issue: $u_{n+1}=U_0+\epsilon\,U_{n+1},\ u_n=U_0+\epsilon U_n, u_{n-1}=U_0+\epsilon U_{n-1}$ following Ref.[44, 45]. Where U_0 is a constant to be determined, $\epsilon\ll 1$ is a small perturbation parameter and U_n is the novel membrane

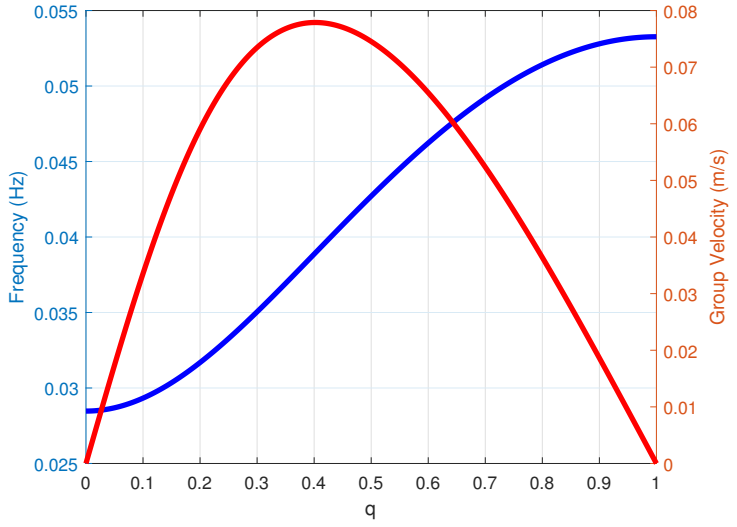

Figure 2: Variation of (a) Frequency $F = \omega_0/2\pi$ and (b) group velocity as function of wave number q using the system parameters: $(a)\ \gamma_0 = 0,\ \gamma_1 = 0.020$, and $(b)\ \gamma_1 = 0.667, D_0 = 0.04, \Omega_0^2 = 0.032$

potential. To advance, we substitute the transformation as thus

$$\begin{aligned}&\epsilon\frac{d^2U_n}{dt^2} + \gamma_1(U_0+\epsilon U_n)^3 + \epsilon(U_0+\epsilon U_n)^2\frac{dU_n}{dt} + {\Omega_0}^2(U_0+\epsilon U_n) + \epsilon\gamma_2\frac{dU_n}{dt}\\ &+\gamma_0 = \epsilon D_0\left(U_{n+1} - 2U_n + U_{n-1}\right) + \epsilon D_1\left(\frac{dU_{n+1}}{dt} - 2\frac{dU_n}{dt} + \frac{dU_{n-1}}{dt}\right)\end{aligned} \tag{4}$$

At order ϵ^0 from Eq.(4), one obtains

$${U_0}^3\gamma_1 + {\Omega_0}^2U_0 + \gamma_0 = 0 \tag{5}$$

Using Eq.(5), the constant U_0 can be readily determined, and by solving the resulting cubic polynomial, one obtains

$$U_0 = -\frac{\sqrt[3]{12}\left({\Omega_0}^2\sqrt[3]{12}\gamma_1 - \left(B{\gamma_1}^2\right)^{2/3}\right)}{6\gamma_1\sqrt[3]{B{\gamma_1}^2}},\quad B = \frac{3(4\,{\Omega_0}^6 + 27\,{\gamma_0}^2\gamma_1)}{\gamma_1} - 9\,\gamma_0, \tag{6}$$

as the only real root for U_0. The remaining two other roots are complex and are ignored. At order ϵ^2, we obtain

$$\begin{aligned}&\frac{d^2U_n}{dt^2} - D_0\left(U_{n+1} - 2U_n + U_{n-1}\right) - D_1\left(\frac{dU_{n+1}}{dt} - 2\frac{dU_n}{dt} + \frac{dU_{n-1}}{dt}\right) + \left(U_n^3\gamma_1 + U_n^2\frac{dU_n}{dt}\right)\epsilon^2\\ &+\left(3U_n\gamma_1 + 2\frac{dU_n}{dt}\right)U_nU_0\epsilon + \left({U_0}^2 + \gamma_2\right)\frac{dU_n}{dt} + \left(3\,{U_0}^2\gamma_1 + {\Omega_0}^2\right)U_n = 0\end{aligned} \tag{7}$$

Eq.(7) is equation of motion and it shall be used to evaluate the impact of potassium leakage current on its control of potassium ion out of the neuron.

3 Dispersion relation and amplitude wave equation

Previously, we have presented the model equation under consideration and derive the modified Liénard equation with the novel membrane potential. Right now, our attention is focused on the derivation of the dispersion relation and schrödinger equation.

3.1 Dispersion relation

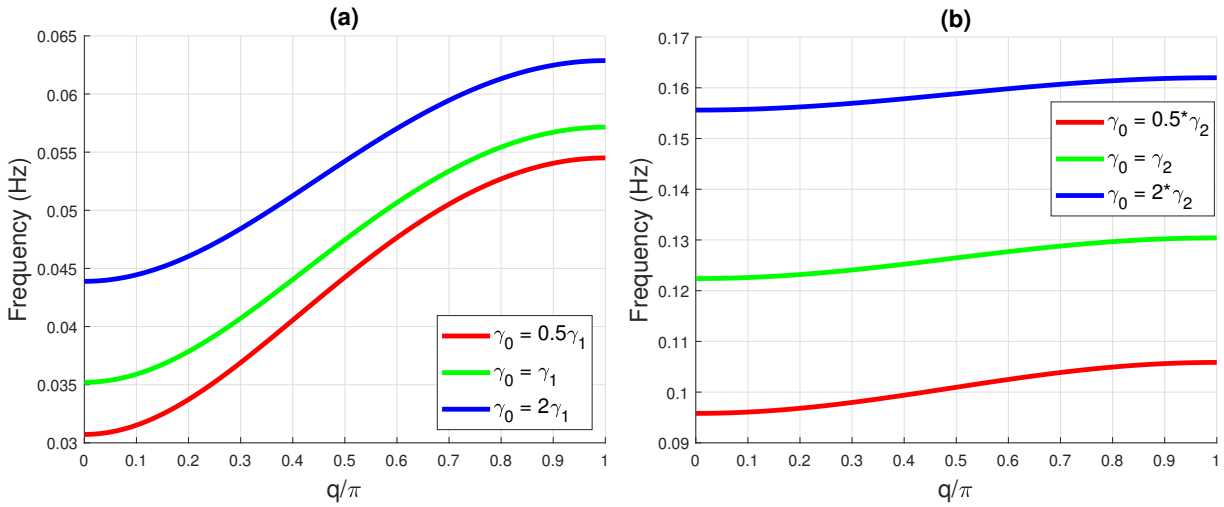

Figure 3: Impact of potassium ions leakage on Frequency $F = \omega_0/2\pi$ as function of wave number q using the system parameters: (a) $\gamma_1 = 0.020$, and (b) $\gamma_1 = 0.667, D_0 = 0.04, \Omega_0^2 = 0.032$

To derive the dispersion relation, we consider a plane wave solution of the form $A_0 \exp(i(nq - \omega t))$ where A_0 represents an infinitesimally small amplitude, ω the angular frequency, We substitute this plane wave solution into Eq.(7), and neglect higher-order terms. This leads us to the dispersion relation as follow

$$\omega^2 = \omega_0 - i\omega_i\omega \tag{8}$$

where

$$\omega_0 = 4D_0 \sin^2\left(\frac{1}{2}q\right) + 3{U_0}^2\gamma_1 + {\Omega_0}^2,\ \omega_i = 4D_1 \sin^2\left(\frac{1}{2}q\right) - \gamma_2 \tag{9}$$

It is observed that the dispersion relation is a complex function and so, any analysis that is done (plotting the graph) is carried out only with the real part. The frequency of the system network is given by, $f = \omega_0/2\pi$, thus a simple analysis of the dispersion relation reveals that the bandwidth of allowed frequencies is given by $[f_0, f_\pi]$ where $f_0 = \sqrt{3{U_0}^2\gamma_1 + {\Omega_0}^2}/2\pi$ and $f_\pi = \sqrt{4D_0 + 3{U_0}^2\gamma_1 + {\Omega_0}^2}/2\pi$ for $q = 0$ and $q = \pi$ respectively. This indicates that the dispersion relation is dependent on the wave number q as seen in Fig.2. As shown in the figure, the frequency increases with the wave number q in solid blue, and illustrates the corresponding variation of the group velocity in solid red. Fig.3 further highlights the influence of potassium ion leakage on the system frequency. It is observed from Fig.3(a) and Fig.3(b) that increasing the leakage-related parameter leads to an increase in the oscillation frequency of the network. This indicates that potassium ion leakage, together with active ionic pumping mechanisms, plays a significant role in modulating the dynamical response of the neuronal system. the group velocity is the first derivative of the dispersion relation with the wave number and by doing so one obtains

$$\mu_0 = \mu_r - i\mu_e \tag{10}$$

where

$$\mu_r = \frac{\sin(q)\, D_0}{\omega}, \quad \mu_e = \sin(q)\, D_1 \tag{11}$$

The graphical representation of the real part of this equation yields the Fig.4. It shows that when $\gamma_0 = 0.01$, the maximum group velocity is $0.077\, m/s$ but when $\gamma_0 = 0.04$, it is noticed that the maximum group velocity is $0.06\, m/s$. Similarly, when $\gamma_0 = 0.333$, the maximum group velocity is about $0.043\, m/s$ for γ_2. These observations from Fig.4(a) and Fig.4(b) indicate that the group velocity decreases as potassium ion leakage increases. This suggests that ionic leakage introduces a dissipative effect that slows down wave propagation in the system, implying an inverse relationship between leakage strength and propagation speed.

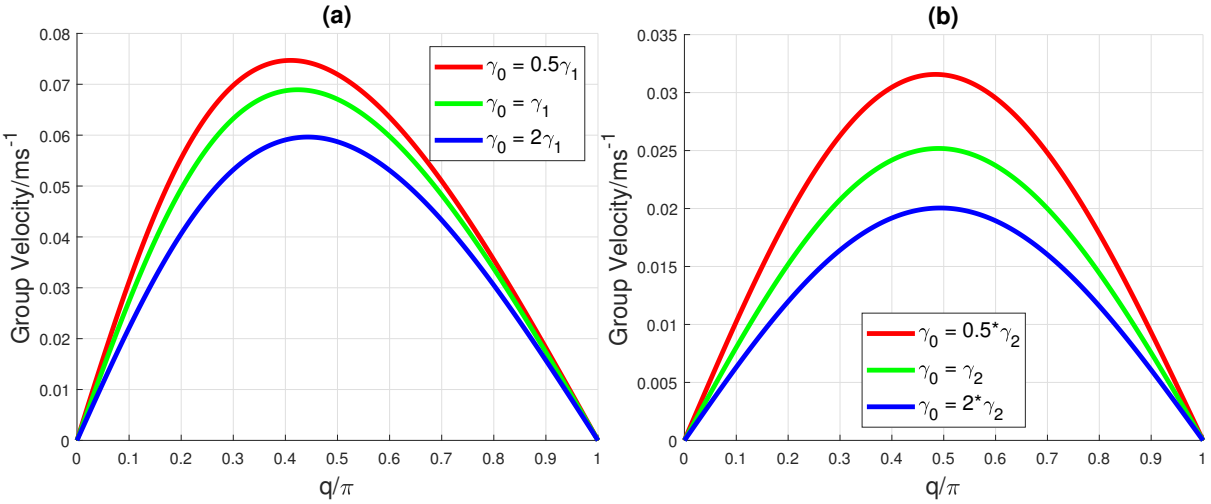

Figure 4: Variation of the real group velocity as function of wave number q using the system parameter for (a) $\gamma_1 = 0.020$, and (b) $\gamma_1 = 0.667, D_0 = 0.04, \Omega_0^2 = 0.032$

3.2 Amplitude wave equation

In this subsection, we focus on deriving an amplitude equation that governs the propagation of modulated waves in the system. For this purpose, the reductive perturbation method is employed, allowing the novel base pairs to be represented through the following asymptotic expansion,

$$U_n(t) = \sum_{j=1}^{2} \epsilon^{j-1} \left[\frac{1}{2} A_{j0}(\xi, \tau) + \sum_{k=1}^{j} A_{jk}(\xi, \tau) e^{ik\theta} \right] + c.c., \tag{12}$$

where,

$$\begin{aligned} \theta &= qn - \omega t, \\ \xi &= \epsilon\,(n - \mu_0 t)\,, \\ \tau &= \epsilon^2 t. \end{aligned} \tag{13}$$

Here, μ_0 denotes the group velocity of the wave in the linear regime. We then seek a solution in powers of ϵ, expressed as a truncated series whose coefficients depend on the variables τ, ξ, and θ.

The imaginary unit is denoted by i, with $i = \sqrt{-1}$. The quantities A_{jk} are complex-valued functions to be determined, and the detailed procedure for obtaining them can be found in [46]. The notation *c.c.* represents the complex conjugate of the preceding terms.

By introducing both fast and slow variables, the time-derivative operator is modified accordingly, as shown in [47, 48, 49].

$$\begin{aligned} \frac{\partial}{\partial t} &= -\epsilon\mu_0 \frac{\partial}{\partial \xi} + \epsilon^2 \frac{\partial}{\partial \tau} - \omega \frac{\partial}{\partial \theta}, \\ \frac{d^2}{dt^2} &= \omega^2 \frac{\partial^2}{\partial \theta^2} + 2\epsilon^2 \omega \frac{\partial^2}{\partial \tau \partial \theta} + ..., \end{aligned} \tag{14}$$

Upon substituting these expressions into (7) and performing routine algebraic manipulations, the following results are obtained.

At order ϵ^0 from $\exp(i0\theta)$, one gets

$$A_{10} = -\frac{U_0^2}{3U_0^2\gamma_1 + \Omega_0^2} \tag{15}$$

The terms of order ϵ proportional to $\exp(0i\theta)$ and $\exp(2i\theta)$ respectively are given by

$$A_{20} = R_1 |A_{11}|^2 \tag{16}$$

$$A_{22}(\xi, \tau) = (\eta_0 + i\eta_i)\, A_{11}^2(\xi, \tau) \tag{17}$$

From the terms of order ϵ^2, proportional to $\exp(i\theta)$, we obtain:

$$(i + \lambda_0) \frac{\partial A_{11}}{\partial \tau} + (P + iP_r) \frac{\partial^2 A_{11}}{\partial \xi^2} + (Q + iQ_r) |A_{11}|^2 A_{11} + (R + iR_r) A_{11} = 0 \tag{18}$$

where

$$\eta_0 = -\frac{U_0}{\begin{array}{l} -64\cos(2q)\cos(q)\,\omega^2 D_1^2 + 16\cos(2q)\,\omega^2 D_1\gamma_2 \\ +36\cos(2q)D_0U_0^2\gamma_1 - 32\cos(q)\,\omega^2 D_1\gamma_2 + 9\Omega_0^4 \\ +81U_0^4\gamma_1^2 + 16\omega^2 D_1^2 + 4\omega^2\gamma_2^2 + 36D_0\Omega_0^2 \\ +4\cos^2(2q)D_0^2 + 64\cos^2(q)D_0^2 + 24\cos(2q)D_0^2 \\ +54\Omega_0^2U_0^2\gamma_1 + 108D_0U_0^2\gamma_1 + 16\omega^2 D_1\gamma_2 \\ +16\cos^2(2q)\,\omega^2 D_1^2 - 32\cos(2q)\cos(q)D_0^2 \\ +64\cos^2(q)\,\omega^2 D_1^2 + 32\cos(2q)\,\omega^2 D_1^2 - 64\cos(q)\,\omega^2 D_1^2 \\ +12\cos(2q)D_0\Omega_0^2 - 48\cos(q)D_0\Omega_0^2 - 96\cos(q)D_0^2 \\ +36D_0^2 - 144\cos(q)D_0U_0^2\gamma_1 \\ \Big(8\cos(2q)\,\omega^2 D_1 - 16\cos(q)\,\omega^2 D_1 + 27U_0^2\gamma_1^2 \\ \times +6\cos(2q)D_0\gamma_1 - 24\cos(q)D_0\gamma_1 + 8\omega^2 D_1 \\ +4\omega^2\gamma_2 + 9\Omega_0^2\gamma_1 + 18D_0\gamma_1\Big) \end{array}} \tag{19a}$$

$$\eta_i = \frac{2\omega U_0}{\begin{array}{l} -64\cos(2q)\cos(q)\,\omega^2 D_1^2 + 16\cos(2q)\,\omega^2 D_1\gamma_2 \\ +36\cos(2q)D_0U_0^2\gamma_1 - 32\cos(q)\,\omega^2 D_1\gamma_2 + 9\Omega_0^4 \\ +81U_0^4\gamma_1^2 + 16\omega^2 D_1^2 + 4\omega^2\gamma_2^2 + 36D_0\Omega_0^2 \\ +4\cos^2(2q)D_0^2 + 64\cos^2(q)D_0^2 + 24\cos(2q)D_0^2 \\ +54\Omega_0^2U_0^2\gamma_1 + 108D_0U_0^2\gamma_1 + 16\omega^2 D_1\gamma_2 \\ +16\cos^2(2q)\,\omega^2 D_1^2 - 32\cos(2q)\cos(q)D_0^2 \\ +64\cos^2(q)\,\omega^2 D_1^2 + 32\cos(2q)\,\omega^2 D_1^2 - 64\cos(q)\,\omega^2 D_1^2 \\ +12\cos(2q)D_0\Omega_0^2 - 48\cos(q)D_0\Omega_0^2 - 96\cos(q)D_0^2 \\ +36D_0^2 - 144\cos(q)D_0U_0^2\gamma_1 \\ \Big(-6\cos(2q)D_1\gamma_1 + 12\cos(q)D_1\gamma_1 + 9U_0^2\gamma_1 \\ \times +2\cos(2q)D_0 - 8\cos(q)D_0 - 6D_1\gamma_1 \\ +3\Omega_0^2 - 3\gamma_1\gamma_2 + 6D_0\Big) \end{array}} \tag{19b}$$

$$\lambda_0 = \frac{2\,\cos(q)\,D_1 - 2\,D_1 - \gamma_2}{2\omega},\ R_1 = -\frac{6U_0\gamma_1}{3U_0^2\gamma_1 + \Omega_0^2} \tag{20a}$$

$$P = \frac{{\mu_e}^2 - {\mu_r}^2}{2\omega},\ P_r = \frac{\mu_e\mu_r}{\omega} \tag{20b}$$

$$Q = -\frac{2\,\omega\,U_0\eta_e + 6\,R_1U_0\gamma_1 + 6\,U_0\eta_0\gamma_1 + 3\,\gamma_1}{2\omega},\ Q_r = \frac{2\,\omega\,R_1U_0 + 2\,\omega\,U_0\eta_0 - 6\,U_0\eta_e\gamma_1 + \omega}{2\omega} \tag{20c}$$

$$R = \frac{3{U_0}^4\gamma_1}{\omega\,\left(9\,{U_0}^4{\gamma_1}^2 + 6\,{\Omega_0}^2{U_0}^2\gamma_1 + {\Omega_0}^4\right)},\ R_r = \frac{{U_0}^4}{9\,{U_0}^4{\gamma_1}^2 + 6\,{\Omega_0}^2{U_0}^2\gamma_1 + {\Omega_0}^4} \tag{20d}$$

Factoring the coefficient of $dA_{11}/d\tau$ and simplifying Eq.(18) results to the cubic complex nonlinear Schrödinger Equation (CNLSE) as shown below.

$$\frac{\partial A_{11}}{\partial \tau} + \alpha\frac{\partial^2 A_{11}}{\partial \xi^2} + \beta|A_{11}|^2A_{11} + \gamma A_{11} = 0 \tag{21}$$

with

$$\begin{aligned}\alpha &= \frac{(P + iP_r)(\lambda_0 - i)}{\lambda_0^2 + 1}\\ \beta &= \frac{(Q + iQ_r)B_{11}(\lambda_0 - i)}{\lambda_0^2 + 1}\\ \gamma &= \frac{(R + iR_r)(\lambda_0 - i)}{\lambda_0^2 + 1}\end{aligned} \tag{22}$$

At this point, the graphical representation of the real expression of the amplitude equation coefficients α, β, γ and $\alpha\beta$ as function of the wave number q are plotted and the curves are shown in Figs:5-8. In these curves, the impact of potassium leakage is evaluated and the general remark shows that the increase of the potassium leakage related-parameter γ_0 decreases the intensity of the constants $\{\alpha, \beta, \gamma, \alpha\beta\}$. The significance to this is simply that the potassium leakage weakens both dispersion and nonlinearity.

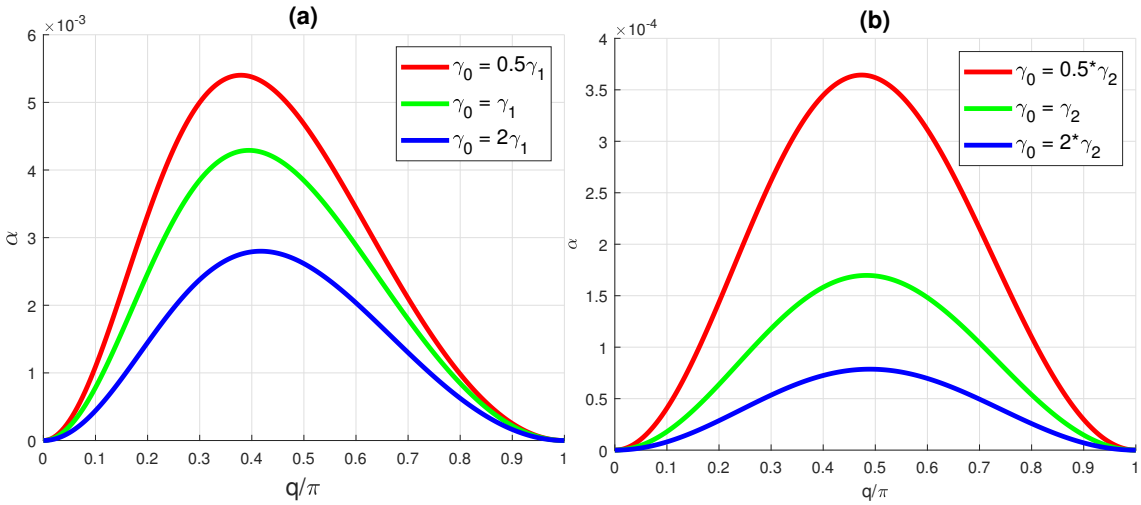

Figure 5: Variation of the real α as function of wave number q showing the impact of γ_0 using the system parameter: (a) $\gamma_1 = 0.020$, and (b) $\gamma_1 = 0.667, D_0 = 0.04, \Omega_0^2 = 0.032$

4 Modulational Instability Analysis (Real Evolution Equation)

Modulational instability (MI) is a fundamental phenomenon in nonlinear wave theory where a uniform (continuous wave) solution becomes unstable under small perturbations, leading to the growth of localized

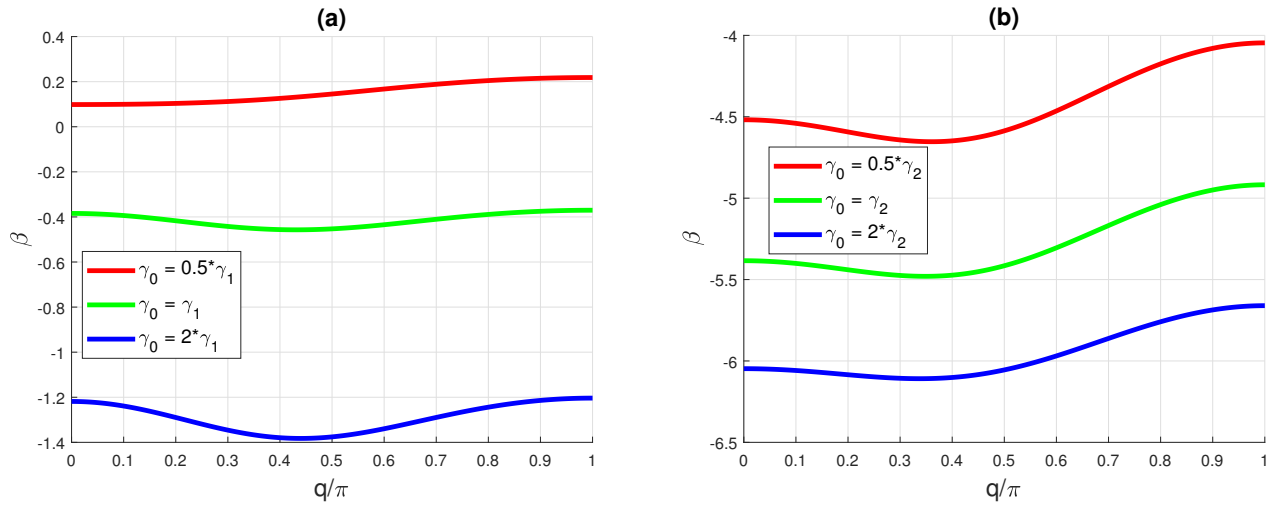

Figure 6: Variation of the real β as function of wave number q showing the impact of γ_0 using the system parameter: (a) $\gamma_1 = 0.020$, and (b) $\gamma_1 = 0.667, D_0 = 0.04, \Omega_0^2 = 0.032$

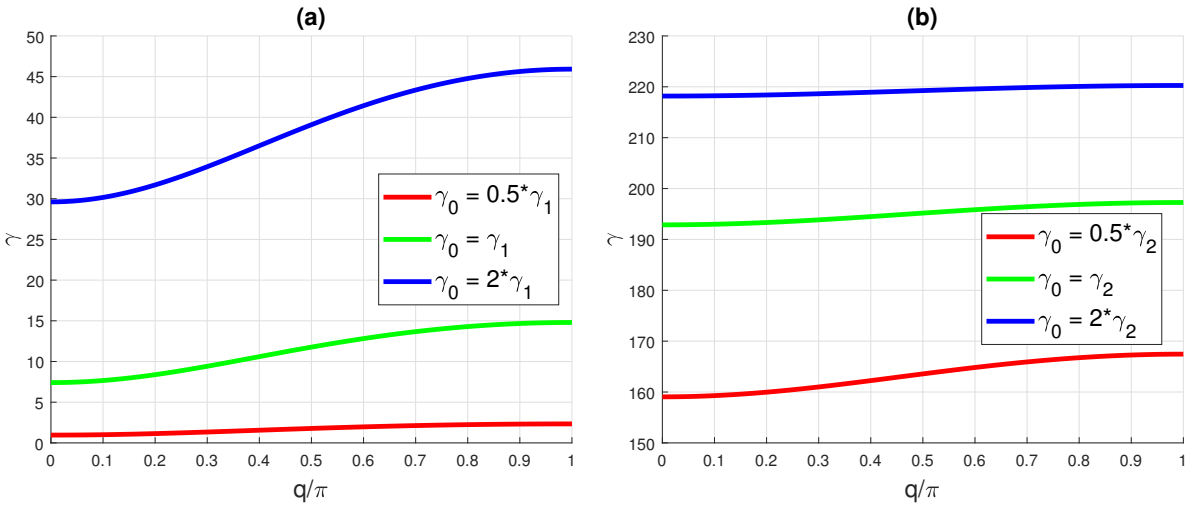

Figure 7: Variation of the real γ as function of wave number q showing the impact of γ_0 using the system parameter: (a) $\gamma_1 = 0.020$, and (b) $\gamma_1 = 0.667, D_0 = 0.04, \Omega_0^2 = 0.032$

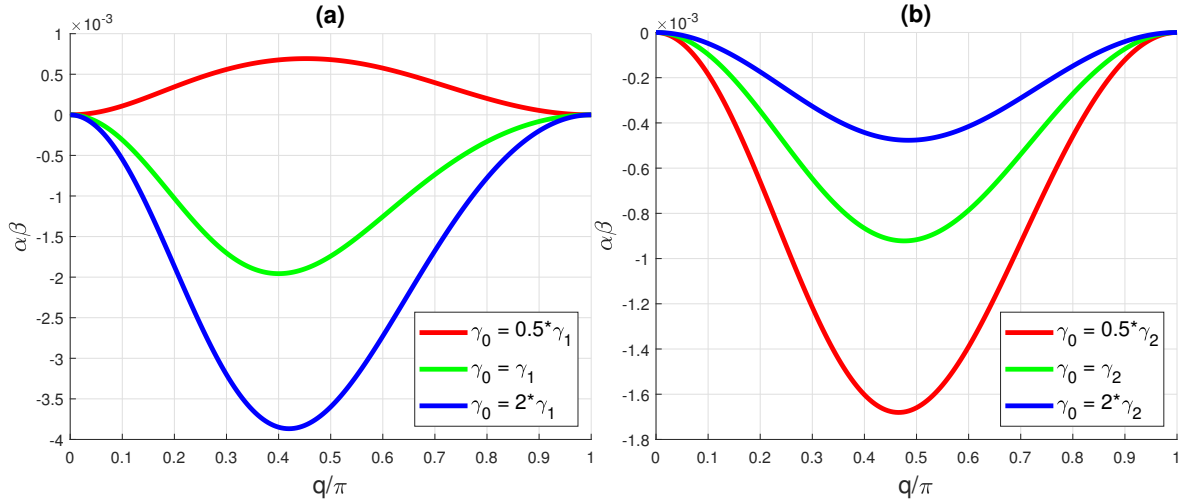

Figure 8: Variation of the real $\alpha\beta$ as function of wave number q showing the impact of γ_0 using the system parameter: (a) $\gamma_1 = 0.020$, and (b) $\gamma_1 = 0.667, D_0 = 0.04, \Omega_0^2 = 0.032$

structures [50, 51].

In systems such as the nonlinear Schrödinger equation (NLSE), modulational instability arises from the interplay between dispersion and nonlinearity. When a small modulation is introduced to a constant-amplitude wave, it can either decay or grow depending on system parameters [52, 53]. We consider Eq.(21) and first look for a continuous wave (CW) solution by assuming that A_{11} is a constant in both space and time, $A_{11} = A_0$. Substituting this into the governing equation yields the algebraic relation $\gamma A_0 + \beta |A_0|^2 A_0 = 0$. For nontrivial solutions ($A_0 \neq 0$), this condition simplifies to

$$\gamma + \beta |A_0|^2 = 0, \tag{23}$$

which defines the amplitude of the steady-state wave in terms of the system parameter. To study the stability of this steady-state solution, we introduce a small perturbation $\epsilon(\xi, \tau)$ superimposed on A_0:

$$A_{11} = A_0 + \epsilon(\xi, \tau), \quad |\epsilon| \ll |A_0|. \tag{24}$$

The goal is to determine whether such perturbations grow or decay over time. Substituting the perturbed solution into the governing equation and keeping only terms linear in ϵ, we obtain.

$$\frac{\partial \epsilon}{\partial \tau} + \alpha \frac{\partial^2 \epsilon}{\partial \xi^2} + (\gamma + 2\beta |A_0|^2)\epsilon + \beta A_0^2 \epsilon^* = 0. \tag{25}$$

Using the steady-state condition $\gamma + \beta |A_0|^2 = 0$, this simplifies further to

$$\frac{\partial \epsilon}{\partial \tau} + \alpha \frac{\partial^2 \epsilon}{\partial \xi^2} + \beta |A_0|^2 \epsilon + \beta A_0^2 \epsilon^* = 0. \tag{26}$$

The star $*$ denotes the complex conjugates of ϵ Normal mode analysis of the last equation, allows us to assume perturbations take the form of plane waves:

$$\epsilon = a e^{iK_0 \xi + \lambda \tau} + b^* e^{-iK_0 \xi + \lambda \tau}. \tag{27}$$

where K_0 is the wavenumber of the perturbation, λ is the growth rate, and a, b are small complex amplitudes. Substituting this form into the linearized equation gives the dispersion relation Substituting into the linearized system yields the dispersion relation (see Appendix A).

$$\lambda^2 = K_0^2 \alpha \left(\alpha K_0^2 + 2\beta |A_0|^2 \right). \tag{28}$$

The growth rate of small perturbations is given by the square-root of Eq.(27) and depending on the sign of λ^2, we distinguish three case study:

- **Case 1:** $\lambda > 0$

When λ is real and positive, small perturbations grow exponentially in time. This corresponds to *modulational instability*, leading to the formation of localized structures such as *bright solitons* or energy focusing regions. This occurs typically when the product $\alpha\beta < 0$ for certain wavenumbers K_0.

- **Case 2:** $\lambda = 0$

  When $\lambda = 0$, the perturbation neither grows nor decays. The wave is neutrally stable at that particular wavenumber. This corresponds to a *marginally stable* mode, where the system may support persistent oscillatory modulations without amplification or decay. At this stage we obtain a critical wavenumber of the perturbation as

$$K_0^2 = -\frac{2\beta|A_0|^2}{\alpha} \tag{29}$$

- **Case 3:** $\lambda < 0$

  If λ is purely imaginary (i.e., $\lambda^2 < 0$), perturbations do not grow exponentially but instead oscillate in time. Physically, this represents *stable modes*, where the wave remains bounded and modulational instability does not occur.

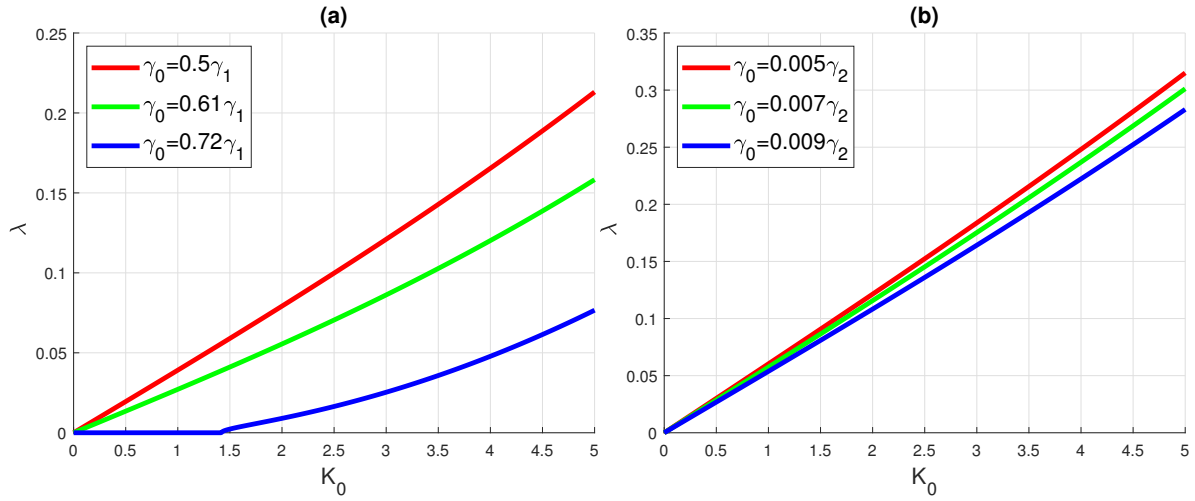

Figure 9: Impact of γ_0 on the growth rate as function of wavenumber K_0 using the network parameters

This behavior is consistent with the modulational instability growth rate shown in Fig.9. Figure.9(a) and Fig.9(b) all show that the growth rate λ decreases when γ_0 increases meaning leakages suppress modulational instability. In other words, potassium leakage acts as a stabilizing dissipative mechanism that suppresses the growth of perturbation and limit energy localization

5 Exact solitary wave solution

In the preceding analysis, a discrete nonlinear differential equation was first derived, after which the coupled nonlinear Schrödinger (CNLS) equation was formulated via the standard reductive perturbation method. In the present section, we examine the propagation of exact solitary wave solutions in a dissipative myelinated axon, with particular emphasis on the role of potassium ion leakage. To construct analytical solitary wave

solutions of Eq. (21), we adopt the method described in Refs. [44, 45, 54] and assume a solution of the form

$$A_{11}(\xi,\tau) = f(\xi,\tau)e^{i(\kappa\xi-\Omega\tau)} \tag{30}$$

where $f(\xi,\tau)$ is real-valued function to be determined, while κ and Ω are arbitrary real constants representing the wave number and frequency shift, respectively. Substituting this ansatz into the CNLSE given in Eq. (21) and introducing the travelling wave transformation $z = \xi - v\tau$, we separate the resulting expression into its real and imaginary components. This procedure yields the following coupled system of ordinary differential equations:

$$\alpha\frac{d^2f}{dz^2} - v\frac{df}{dz} + \beta f^3 + \left(\gamma - \alpha\,\kappa^2\right) f = 0 \tag{31a}$$

$$2\alpha\,\kappa\frac{df}{dz} - \Omega f = 0 \tag{31b}$$

To preserve the localized solitary wave structure of the solution, we eliminate the first-order derivative term of f with respect to z in Eq. (31a). This is achieved by expressing $\frac{df}{dz}$ from Eq. (31b) and substituting it back into Eq. (31a), thereby reducing the system to a single nonlinear evolution equation. As a result, the governing equation takes the form of a cubic Duffing-type oscillator given by

$$\frac{d^2f}{dz^2} = q_2 f - q_1 f^3 \tag{32}$$

where

$$q_1 = \frac{\beta}{\alpha},\;\; q_2 = -\frac{-2\,\alpha^2\kappa^3 + 2\,\alpha\,\gamma\,\kappa - \Omega\,v}{2\alpha^2\kappa} \tag{33}$$

which clearly show the dependence of the effective nonlinear and dispersive parameters on the system characteristics.

5.1 Dynamical analysis

A deeper qualitative understanding of the solution behavior can be obtained through a dynamical systems approach. Accordingly, the Duffing-type oscillator in Eq. (32) is reformulated as the first-order system

$$\frac{df}{dz} = \rho, \qquad \frac{d\rho}{dz} = q_2 f - q_1 f^3 \tag{34}$$

where ρ represents the auxiliary phase variable associated with the evolution of f. By direct integration, the system admits the first integral

$$H(\rho, f) = \rho^2 - q_2 f^2 + \frac{q_1}{2} f^4 = C_i \tag{35}$$

where C_i is an integration constant determined by initial or boundary conditions.

The dynamical behavior of system (34) is notably rich and highly sensitive to parameter variations,

since the coefficients q_1 and q_2 depend not only on the intrinsic properties of the CNLS equation but also on external wave parameters such as v, κ, and Ω. In particular, q_2 exhibits strong parametric sensitivity and can be tuned through suitable adjustments of these quantities, thereby controlling the nature of the resulting wave structures. As an illustration, q_2 vanishes when the wave velocity v satisfies the critical condition.

$$v = \frac{2\alpha\left(\gamma - \alpha\,\kappa^2\right)\kappa}{\Omega} \tag{36}$$

To proceed further, we impose the condition $H(\rho, f) = C_i = 0$, which is physically motivated by the restriction to the regime dominated by potassium ion leakage effects. Under this assumption, Eq. (35) reduces to

$$\frac{df}{dz} = \sqrt{q_2 f^2 - \frac{q_1}{2} f^4} \tag{37}$$

which governs the spatial evolution of the solitary wave profile. Rearranging this expression leads to the integral form

$$\sqrt{q_2}z = \int \frac{df}{f\sqrt{1 - \frac{q_1}{2q_2} f^2}} \tag{38}$$

which provides the basis for obtaining a family of exact analytical solutions under different boundary conditions and parameter regimes, thereby revealing a variety of possible solitary wave structures.

5.2 Bright soliton

We now focus on deriving a bright solitary wave solution. In this case, we introduce an appropriate change of variables to facilitate the integration of the above expression, allowing the integral to be evaluated more straightforwardly as follows, $f(z) = \sqrt{\frac{2q_2}{q_1}}\mathrm{sech}(\theta)$ and the condition to achieve is the product of $\alpha\beta < 0$. Substituting this setting appropriately and simplify results to $\theta = \sqrt{q_2}z$. This implies that the solution is given by

$$f(z) = A_0\,\mathrm{sech}(\sqrt{q_2}z) \tag{39}$$

where $A_0 = \sqrt{\frac{2q_2}{q_1}}$. With Eq.(30), the bright soliton amplitude is then given by:

$$A_{11} = A_0\,\mathrm{sech}(\sqrt{q_2}z)e^{i(\kappa\xi - \Omega\tau)}. \tag{40}$$

The bright soliton profile is presented in Fig.10, where the effect of potassium ion leakage is examined. The results indicate that for a leakage parameter of 0.01, the squared amplitude of the bright soliton is approximately $80\,\mathrm{m}^2$. When the level of ionic leakage is quadrupled, the squared amplitude increases significantly to about $122\,\mathrm{m}^2$. These results clearly demonstrate that the soliton intensity is strongly modulated by ionic leakage. In other words, an increase in potassium leakage leads to a corresponding enhancement of the bright soliton amplitude. The final solution for the new membrane potential after substituting Eq.(43) back

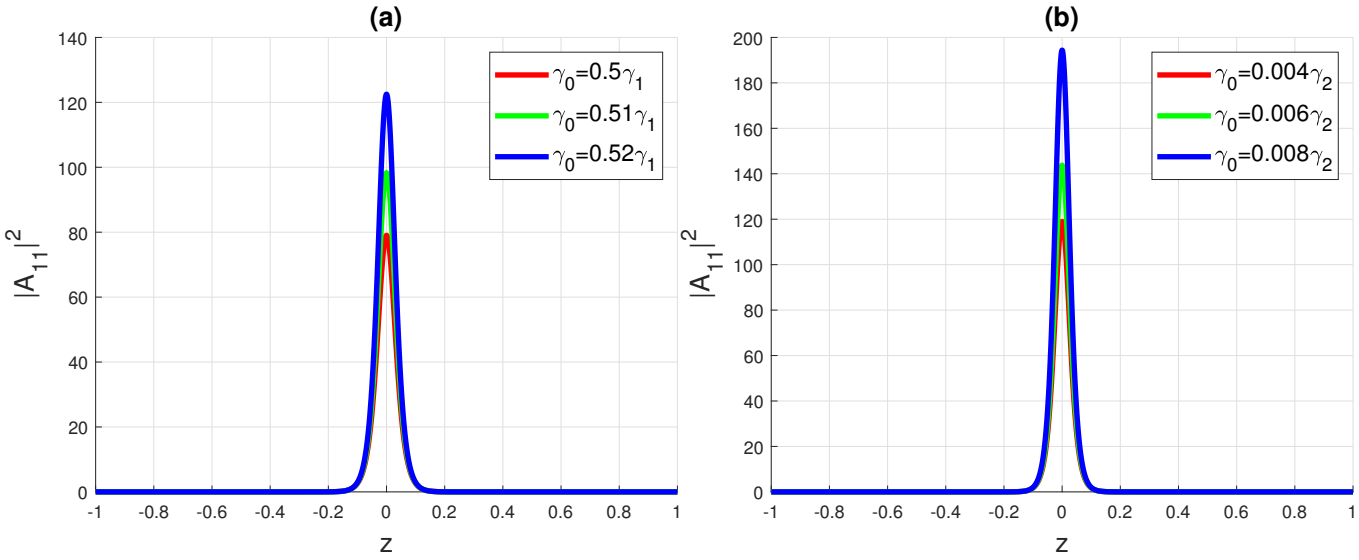

Figure 10: Impact of the parameter γ_0 on the bright soliton with respect to z using system parameter

into Eq.(12) yields

$$U_n(t) = -\frac{{U_0}^2}{3\,{U_0}^2\gamma_1 + {\Omega_0}^2} + 2\sqrt{\frac{2q_2}{q_1}}\operatorname{sech}(\sqrt{q_2}z)\cos(\Phi) + \frac{2\epsilon q_2}{q_1}\operatorname{sech}^2(\sqrt{q_2}z)\,(R_1 + 2\eta_1\cos(2\Phi)) \tag{41}$$

with $\Phi = \Omega\tau - \kappa\xi - \theta$ and $z = \xi - v\tau$

5.3 Dark soliton

Once again, our objective is to derive a dark solitary wave solution. To achieve this, we introduce a suitable change of variables that simplifies the integration of the above expression, allowing the integral to be evaluated more conveniently as follows, $f(z) = \sqrt{\frac{2q_2}{q_1}}\tanh(\theta)$ making sure that $\alpha\beta > 0$. Substituting this setting appropriately and simplify results to $\theta = \sqrt{q_2}z$. This implies that the solution is given by

$$f(z) = A_0\tanh(\sqrt{q_2}z) \tag{42}$$

where $A_0 = \sqrt{\frac{2q_2}{q_1}}$. The condition for dark soliton to occur is that the sign With Eq.(42), the dark soliton amplitude is then given by:

$$A_{11} = A_0\tanh(\sqrt{q_2}z)e^{i(\kappa\xi - \Omega\tau)}. \tag{43}$$

The dark soliton equation is graphically represented in Fig. 11, where the effect of potassium leakage is examined. The results indicate that as the potassium leakage increases, the squared amplitude of the dark soliton decreases to lower values. Hence, the soliton intensity is inversely proportional to γ_0 The final solution for the new membrane potential after substituting Eq.(43) back into Eq.(12) yields

$$U_n(t) = -\frac{{U_0}^2}{3\,{U_0}^2\gamma_1 + {\Omega_0}^2} + 2\sqrt{\frac{2q_2}{q_1}}\tanh(\sqrt{q_2}z)\cos(\Phi) + \frac{2\epsilon q_2}{q_1}\tanh^2(\sqrt{q_2}z)\,(R_1 + 2\eta_1\cos(2\Phi)) \tag{44}$$

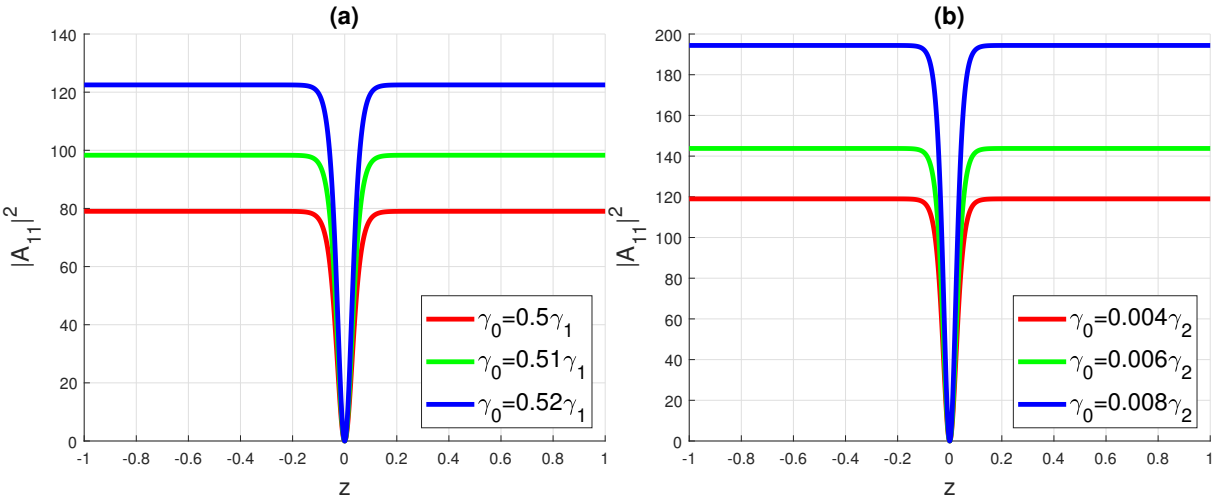

Figure 11: Impact of the parameter γ_0 on the dark soliton with respect to z using system parameter

5.4 Periodic solution

Periodic solutions refer to solutions of differential equations whose values recur after a fixed interval, known as the period. They characterize oscillatory or wave-like behaviors that frequently arise in physical, biological, and engineering systems. These solutions are essential for analyzing long-term dynamics, stability properties, and pattern formation in nonlinear systems. The periodic solution of Eq. (38) is obtained as follows.

$$f(z) = A\,\mathrm{sn}(Bz, m) \tag{45}$$

where

$$\begin{aligned} B &= \sqrt{A^2 b + a}, \\ a &= (\gamma - \alpha\kappa^2 + i\Omega)/\alpha - \lambda_0^2, \\ b &= \beta/\alpha, \\ m &= (bA^2)/2B \end{aligned} \tag{46}$$

The graphical representation of the periodic solution is given in Fig.12. In Fig.12a, γ_0 is adjusted such that the value of m is less than unit to obtain the curve given by it. However, in Fig.10b, γ_0 is modified so as to have $m = 0$. What is seen is no longer a periodic solution but a soliton-like solution. This corresponds to a kink-type or anti-kink solitary structure solitary wave solution.

6 Numerical solution

Formerly, we have established the analitical solution. In this section, we focus on numerical analysis of the paper. The numerical simulation of lattice solitons was performed on a one-dimensional discrete lattice with N sites. The fixed parameters include the lattice wavenumber q, coupling constants D_0 and D_1, nonlinear coefficients γ_1 and γ_2, a small perturbation ϵ, and the base frequency squared Ω_0^2. The values of these fixed

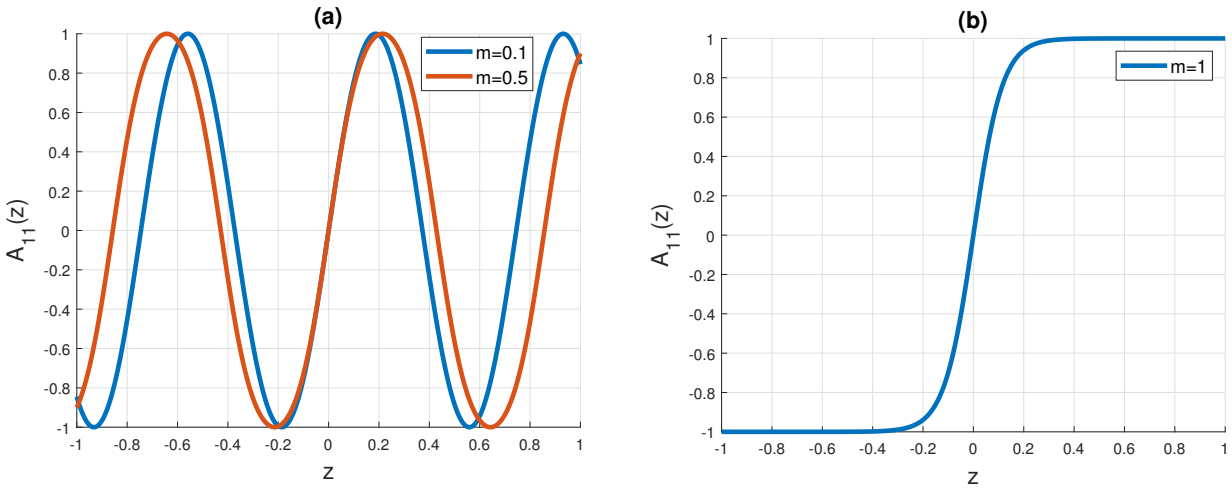

Figure 12: Graphical representation of the periodic solution as function of z, for different m using the system parameter. (a) $0 < m < 1$ (b) m=1 as

constants are: $q = 0.1\pi, \gamma_1 = 0.020, \gamma_2 = 0.667, D_0 = 0.020, D_1 = 0.001, \Omega_0^2 = 0.032$ [36, 37]. The constant U_0 and linear real frequency ω_0 were computed from these constants, incorporating both nonlinear and dispersive effects of the lattice.

The governing nonlinear lattice equation (7) was discretized using finite differences as,

$$\begin{aligned} &D_0\left(2U_n^k - U_{n+1}^k - U_{n-1}^k\right) + D_1\left[2\frac{U_n^{k+1}-U_n^k}{\Delta t} - \frac{U_{n+1}^{k+1}-U_{n+1}^k}{\Delta t} - \frac{U_{n-1}^{k+1}-U_{n-1}^k}{\Delta t}\right] \\ &+ \epsilon^2\left((U_n^k)^3 + U_n^k\frac{U_n^{k+1}-U_n^k}{\Delta t}\right) + \epsilon\left(3(U_n^k)^2U_0\gamma_1 + 2U_n^k\frac{U_n^{k+1}-U_n^k}{\Delta t}U_0\right) \\ &+ (U_0^2+\gamma_2)\frac{U_n^{k+1}-U_n^k}{\Delta t} + \left(3U_0^2\gamma_1 + \Omega_0^2\right)U_n^k + \frac{U_n^{k+1}-2U_n^k+U_n^{k-1}}{(\Delta t)^2} = 0 \end{aligned} \tag{47}$$

and periodic boundary conditions were applied. The initial condition consisted of a localized soliton-like profile (Eq.(41) for bright soliton and Eq.(44) dark soliton) modulated by ϵ, representing a small perturbation (For both bright and dark soliton). Time evolution was computed using an explicit Euler method, with a time span t_{span} discretized into sufficiently small steps to maintain stability. To achieve, we firstly introduce a first-order variable V_n^k since Eq.(7) is second order derivative.

$$V_n^k = \frac{U_n^k - U_n^{k-1}}{\Delta t} \quad \Rightarrow \quad \frac{U_n^{k+1}-U_n^k}{\Delta t} = V_n^{k+1}, \tag{48}$$

Examining all terms at step k including nonlinearities and spatial finite differences results to

$$V_n^{k+1} = V_n^k + \Delta t\, f\left(U_{n-1}^k, U_n^k, U_{n+1}^k, V_{n-1}^k, V_n^k, V_{n+1}^k\right), \tag{49}$$

where $f(\cdot)$ stands for the right-hand side of the original discretized equation. Finally, updating displacement U_n leads to

$$U_n^{k+1} = U_n^k + \Delta t\, V_n^{k+1}. \tag{50}$$

The lattice acceleration at each site was evaluated from nearest-neighbor interactions, nonlinear terms, and contributions from the background amplitude. Velocities and displacements were updated iteratively, generating the soliton dynamics over the temporal domain.

To obtain stable soliton solutions, adjustments of the nonlinear coefficient γ_0 (as multiples of γ_1 or γ_2) and the frequency Ω_0 were performed. The method allows tracking the propagation and evolution of solitons, and results were visualized as three-dimensional surfaces showing the displacement $U_n(t)$ as a function of lattice position and time. Small time steps and careful selection of parameters ensured numerical stability and convergence of the solution. The three-dimensional evolution of the bright solitary wave is presented

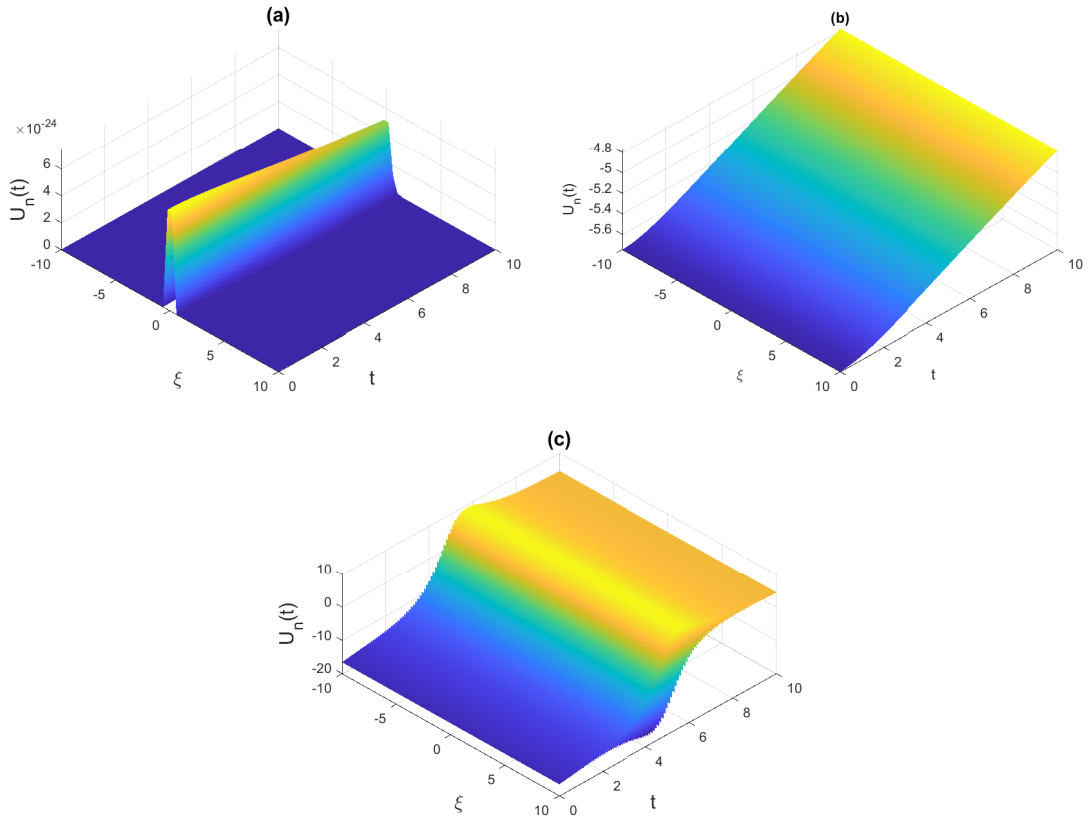

Figure 13: The evolution bright solitary wave in three dimension using system parameter: for (a) $\gamma_0 = 0$, (b) $\gamma_0 = 0.01$,(c) $\gamma_0 = 5$

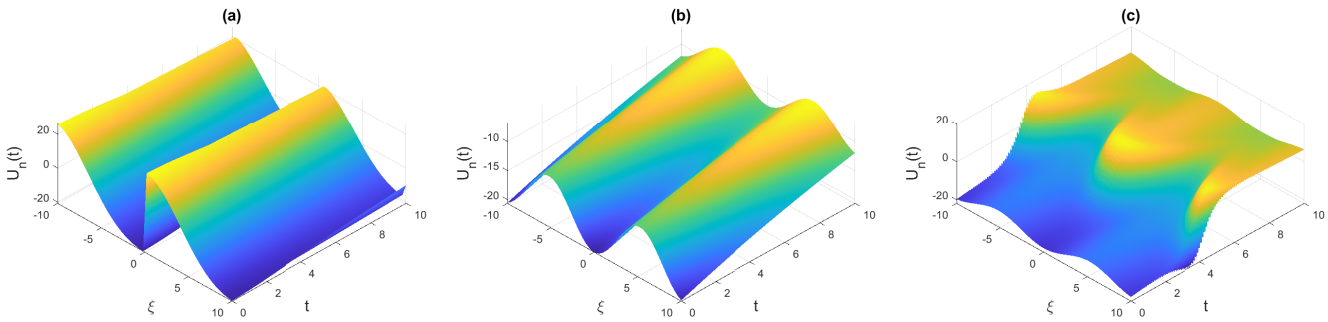

Figure 14: The evolution of dark solitary wave in three dimension using system parameter and with the impact of γ_0 for:(a) $\gamma_0 = 0$,(b)$\gamma_0 = 0.5$,(c)$\gamma_0 = 5$

in Fig.13(a)-13(c). Specifically, Fig.13(a) corresponds to the case without leakage ($\gamma_0 = 0$) while Fig.13(b)

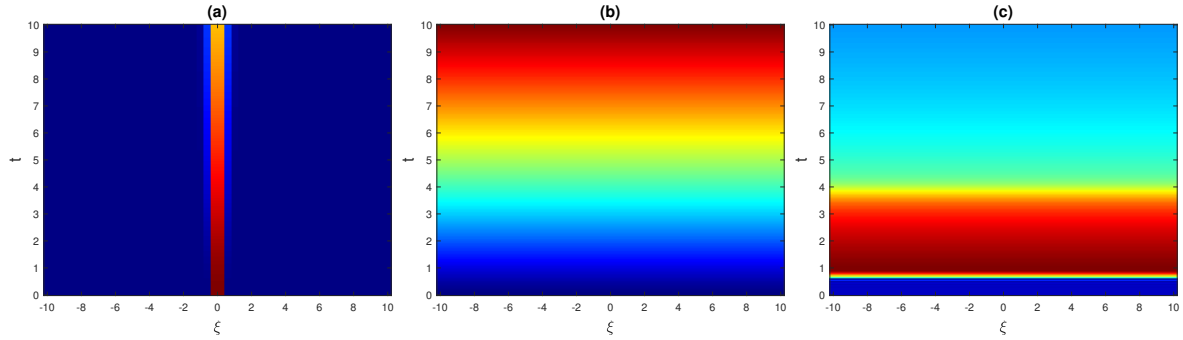

Figure 15: The evolution bright solitary wave in two dimension using system parameter: for (a) $\gamma_0 = 0$, (b) $\gamma_0 = 0.01$,(c) $\gamma_0 = 5$

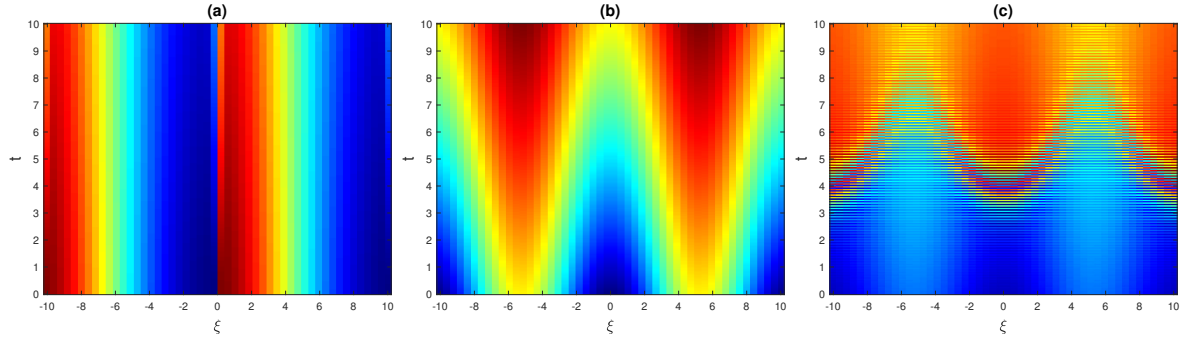

Figure 16: The evolution of dark solitary wave in two dimension using system parameter and with the impact of γ_0 for:(a) $\gamma_0 = 0$,(b)$\gamma_0 = 0.5$,(c)$\gamma_0 = 5$

and Fig.13(c) illustrate the effect of increasing leakage. It is observed that the amplitude and localization of the soliton are significantly modified as γ_0 increase. The corresponding evolution for dark solitons is shown in Fig.14(a)-14(c). As the leakage parameter increases from Fig.14(a) to Fig.14(c), the soliton profile becomes progressively attenuated, confirming that leakage suppresses dark soliton structures. The two-dimensional evolution of the soliton profiles is presented in Fig.15(a-c) and Fig.16(a-c), corresponding to bright and dark solitons, respectively. In both cases, increasing γ_0 leads to a noticeable modification of amplitude and localization, confirming the dissipative role of potassium leakage. With the change of initial solution introduced as

$$U(n) = A_0 \,\mathrm{sech}(A_0\sqrt{\beta/\alpha}(\xi(n) - x0))\cos(k(\xi(n) - x_0)) \tag{51}$$

where $A_0 = 0.5, k = 1, x_0 = 0$ in the first case and $A_0 = 0.5 \times 10^2, k = 1 \times 10^2, x_0 = 0$ in the second case, leads to the following observations. The results corresponding to the initial condition in Eq. (51) are presented in Fig. 17 and Fig. 18. Fig. 17 is obtained for $A_0 = 0.5$ and $k = 1$, showing a well-localized wave structure. In contrast, Fig. 18 corresponds to the scaled parameters $A_0 = 0.5 \times 10^2$ and $k = 1 \times 10^2$, where a significant attenuation of the wave amplitude is observed. This clearly highlights the sensitivity of the system to the initial excitation conditions. The inclusion of Fig. 17 and Fig. 18 is important as it provides additional validation of the numerical model under different initial excitations. While previous figures focus on the role of potassium leakage on soliton evolution, these figures demonstrate that the

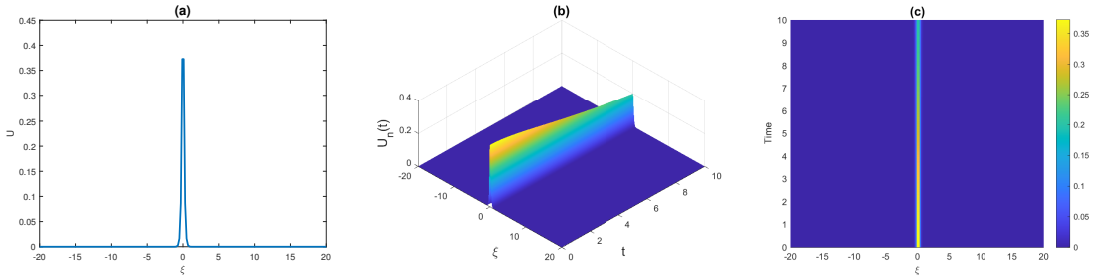

Figure 17: Localized wave profile obtained from Eq. (51) with $A_0 = 0.5$ and $k = 1$, using the fixed system parameters $q = 0.1\pi$, $\gamma_1 = 0.020$, $\gamma_2 = 0.667$, $D_0 = 0.020$, $D_1 = 0.001$, and $\Omega_0^2 = 0.032$.

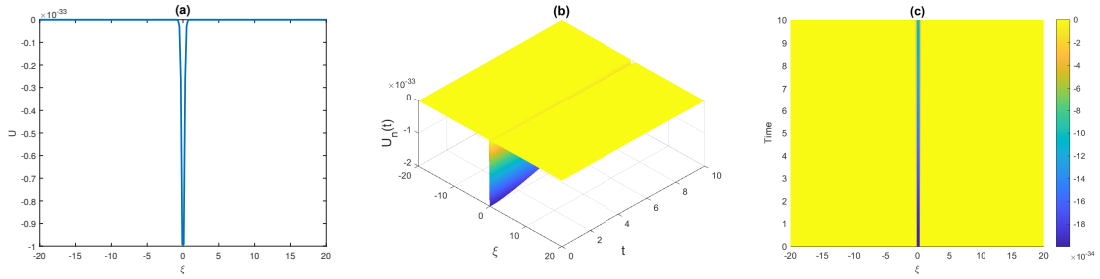

Figure 18: Localized wave profile obtained from Eq. (51) with scaled parameters $A_0 = 0.5 \times 10^2$ and $k = 1 \times 10^2$. The strong attenuation of the wave amplitude demonstrates the sensitivity of the system to initial condition scaling.

formation, amplitude, and localization of nonlinear waves also depend strongly on the initial conditions. This confirms that both system parameters and initial excitation jointly govern the observed dynamics. Overall, numerical simulations validate the theoretical predictions and demonstrate that potassium leakage significantly modifies both the amplitude and propagation dynamics of nonlinear waves. These results confirm that increasing potassium leakage leads to slower, more localized, and more stable wave structures, in excellent agreement with analytical predictions.

7 Conclusions

In this study, we examined the influence of potassium ion leakage on a myelinated dissipative axon. We began by introducing the Liénard-type model and subsequently derived the corresponding equation of motion that explicitly incorporates the leakage effect, a parameter often neglected in previous studies.

Next, we established the dispersion relation and the associated group velocity. At this stage, the role of potassium ion leakage was carefully analyzed, revealing its noticeable impact on the wave dynamics. Building on this, we derived the governing amplitude equation, which takes the form of a cubic complex Nonlinear Schrödinger Equation (CNLSE). Additionally, the influence of the parameter γ_0 on the CNLSE coefficients was investigated, and the resulting behavior provided valuable insights. A modulational instability analysis was then performed, showing that the growth rate of perturbations depends both on their wavenumber and on the potassium ion leakage.

Furthermore, we constructed several classes of exact solutions, including bright solitons, dark solitons, and periodic wave structures, obtained by directly integrating Eq.(38). For each solution type, the effect of

potassium ion leakage was systematically examined, yielding physically meaningful and significant results.

Finally, numerical simulations were carried out, and the outcomes showed excellent agreement with the analytical solutions, thereby confirming the robustness and consistency of the analysis.

8 Appendix A: Explicit derivation of λ

In part we try to explicitly show how the growth rate is obtained. To begin, we substitute Eq.(27) back into (26) resulting to

$$\begin{aligned}
&\frac{\partial \epsilon}{\partial \tau} = \lambda a e^{iK_0\xi+\lambda\tau} + \lambda b^* e^{-iK_0\xi+\lambda\tau},\\
&\frac{\partial^2 \epsilon}{\partial \xi^2} = -K_0^2 a e^{iK_0\xi+\lambda\tau} - K_0^2 b^* e^{-iK_0\xi+\lambda\tau},\\
&\beta A_0^2 \epsilon^* = \beta A_0^2 \left(a^* e^{-iK_0\xi+\lambda\tau} + b e^{iK_0\xi+\lambda\tau}\right),\\
&\beta |A_0|^2 \epsilon = \beta |A_0|^2 \left(a e^{iK_0\xi+\lambda\tau} + b^* e^{-iK_0\xi+\lambda\tau}\right)
\end{aligned} \tag{52}$$

and grouping terms in $e^{\pm iK_0\xi}$ gives the system

$$\begin{aligned}
&(\lambda - \alpha K_0^2 + \beta |A_0|^2) a + \beta A_0^2 b = 0,\\
&\beta (A_0^*)^2 a + (\lambda - \alpha K_0^2 + \beta |A_0|^2) b = 0
\end{aligned} \tag{53}$$

Now, applying the nontrivial solution condition (determinant= 0),

$$\begin{vmatrix}
\lambda - \alpha K_0^2 + \beta |A_0|^2 & \beta A_0^2 \\
\beta (A_0^*)^2 & \lambda - \alpha K_0^2 + \beta |A_0|^2
\end{vmatrix} = 0 \tag{54}$$

and solving for λ to obtain the dispersion yields

$$(\lambda - \alpha K_0^2 + \beta |A_0|^2)^2 - \beta^2 |A_0|^4 = 0 \quad \Rightarrow \quad \lambda^2 = \left(\alpha^2 K_0^2 + 2\alpha\beta |A_0|^2\right) K_0^2 \tag{55}$$

CRediT authorship contribution statement

Arnaud Djine: Did the calculations, report and proposed topic. **Serge Bruno Yamgoué**: Checked the calculations, Carried out the numerical analysis, Contributed to the editing.

Declaration of competing interest

The authors declare that they have no known competing financial interests or personal relationships that could have appeared to influence the work reported in this paper.

Data availability

No data was used for the research described in the article.

Funding Declaration

No funding was received for this research

References

[1] J. D. Murray, Mathematical Biology I: An Introduction (Springer, 2002).

[2] S. H. Strogatz, Nonlinear Dynamics and Chaos (Westview Press, 2015).

[3] A. T. Winfree, The Geometry of Biological Time (Springer, 2001).

[4] I. R. Epstein and J. A. Pojman, An Introduction to Nonlinear Chemical Dynamics (Oxford University Press, 1998).

[5] A. M. Turing, Philos. Trans. R. Soc. B 237, 37–72 (1952).

[6] P. C. Fife, Mathematical Aspects of Reacting and Diffusing Systems (Springer, 1979).

[7] R. FitzHugh, Biophys. J. 1, 445–466 (1961).

[8] J. Nagumo, S. Arimoto, and S. Yoshizawa, Proc. IRE 50, 2061–2070 (1962).

[9] A. L. Hodgkin and A. F. Huxley, J. Physiol. 117, 500–544 (1952).

[10] J. Keener and J. Sneyd, Mathematical Physiology (Springer, 1998).

[11] J. P. Keener, SIAM J. Appl. Math. 47, 556–572 (1987).

[12] T. Erneux and G. Nicolis, Physica D 67, 237–244 (1993).

[13] S. Shahid, M. Abbas, and E. Kwessi, Symmetry 16, 585 (2024).

[14] D. A. Koç, Mathematics 14, 795 (2026).

[15] M. Y. Almusawa, K. Aldawsari, and N. Mshary, Bound. Value Probl. 2025, 127 (2025).

[16] E. R. Kandel, J. H. Schwartz, and T. M. Jessell, Principles of Neural Science (McGraw-Hill, 2000).

[17] J. Keener and J. Sneyd, Mathematical Physiology (Springer, 2001).

[18] W. A. H. Rushton, J. Physiol. 115, 101–122 (1951).

[19] B. Hille, Ion Channels of Excitable Membranes (Sinauer, 2001).

[20] S. Flach and A. V. Gorbach, Phys. Rep. 467, 1–116 (2008).

[21] V. Booth and T. Erneux, SIAM J. Appl. Math. 55, 1372–1389 (1995).

[22] A. Carpio and L. L. Bonilla, Phys. Rev. Lett. 86, 6034–6037 (2001).

[23] S. P. Hastings and X. Chen, J. Math. Biol. 38, 1–20 (1999).

[24] D. Luo, C. Wang, Q. Deng, and Y. Sun, Nonlinear Dyn. 113, 5811–5824 (2025).

[25] I. H. Jebril, M. A. Al-Smadi, S. Momani, and others, AIP Conf. Proc. 3338, 040025 (2025).

[26] H. Lodish, A. Berk, C. A. Kaiser, M. Krieger, A. Bretscher, H. Ploegh, A. Amon, and K. C. Martin, Molecular Cell Biology (W. H. Freeman, 2000).

[27] G. Nicolis and I. Prigogine, Self-Organization in Nonequilibrium Systems (Wiley, 1977).

[28] H. Haken, Synergetics (Springer, 1983).

[29] Y. Kuramoto, Chemical Oscillations, Waves, and Turbulence (Springer, 1984).

[30] J. Y. Wu, L. Guan, and Y. Tsau, J. Neurosci. 19, 5005–5015 (1999).

[31] J. D. Murray, Mathematical Biology II (Springer, 2002).

[32] Y. Lu, Y. Sato, and S. Amari, Neural Comput. 23, 1248–1260 (2011).

[33] W. Chang, A. Ankiewicz, and N. Akhmediev, Phys. Rev. A 78, 023830 (2008).

[34] A. M. Dikande and G. A. Bartholomew, Phys. Rev. E 80, 041904 (2009).

[35] G. Zangari del Balzo, Theor. Biol. Med. Model. 18, 1 (2021).

[36] N. O. Nfor and M. T. Mokoli, J. Mod. Phys. 7, 1166–1180 (2016).

[37] N. O. Nfor, P. G. Ghomsi, and F. M. M. Kakmeni, Chin. Phys. B 32, 020504 (2023).

[38] N. O. Nfor, P. G. Ghomsi, and F. M. Moukam Kakmeni, Phys. Rev. E 97, 022214 (2018).

[39] C. Koch, Biophysics of Computation: Information Processing in Single Neurons (Oxford University Press, 1999).

[40] F. M. M. Kakmeni, E. M. Inack, and E. M. Yamakou, Phys. Rev. E 89, 052919 (2014).

[41] S. N. Pandey, P. S. Bindu, M. Senthilvelan, and M. Lakshmanan, J. Math. Phys. 50, 102701 (2009).

[42] D. Banerjee and J. K. Bhattacharjee, J. Phys. A 43, 062001 (2010).

[43] M. Messias and M. R. A. Gouveia, Physica D 240, 1402–1409 (2011).

[44] A. Djine, S. B. Yamgoué, and N. O. Nfor, Braz. J. Phys. 56, 1–17 (2026).

[45] A. Djine, G. R. Deffo, and S. B. Yamgoué, Chaos Solitons Fractals 194, 116178 (2025).

[46] G. R. Deffo, S. B. Yamgoué, T. Fonzin-Fozin, and F. B. Pelap, Chaos Solitons Fractals 144, 110630 (2021).

[47] G. R. Deffo, S. B. Yamgoué, and F. B. Pelap, Phys. Rev. E 98, 062201 (2018).

[48] G. R. Deffo, S. B. Yamgoué, and F. B. Pelap, Phys. Rev. E 100, 022214 (2019).

[49] A. Djine, N. O. Nfor, G. R. Deffo, and S. B. Yamgoué, Chaos Solitons Fractals 181, 114706 (2024).

[50] T. B. Benjamin and J. E. Feir, J. Fluid Mech. 27, 417–430 (1967).

[51] V. E. Zakharov and L. A. Ostrovsky, Physica D 238, 540–548 (2009).

[52] A. Hasegawa and F. Tappert, Appl. Phys. Lett. 23, 142–144 (1973).

[53] M. J. Ablowitz, Nonlinear Dispersive Waves (Cambridge University Press, 2011).

[54] A. Djine, G. R. Deffo, and S. B. Yamgoué, Chaos Solitons & Fractals 170, 113334 (2023).